Energy Band Calculation of $Si/Si_{0.7}Ge_{0.3}$ Nanopillars in $\vec{k}$ Space

Min-Hui Chuang
Parallel and Scientific Computing Laboratory
Institute of Communications Engineering
National Chiao Tung University
Hsinchu City, Hsinchu 300, Taiwan

Yiming Li
Parallel and Scientific Computing Laboratory
Institute of Communications Engineering
National Chiao Tung University
Hsinchu City, Hsinchu 300, Taiwan
ymli@faculty.nctu.edu.tw

***Abstract*—In this work, we explore the energy band of the well-aligned silicon (Si) nanopillars (NPs) embedded in $Si_{0.7}Ge_{0.3}$ matrix fabricated by neutral beam etching. Instead of real-space modeling, we formulate and solve the Schrödinger equation with an effective mass approach using 3D finite-element simulation in $\vec{k}$ space. This approach enables us to calculate the electronic structure in a computationally effective manner. The effects of the height, radius, separation, and shape of Si NPs on the energy band and density of states are calculated and discussed. The effect of the radius on the electron energy band control is significant while that of the shape is marginal owing to high geometry aspect ratio. In contrast with the results of electrons, both the radius and separation play crucial role in tuning the energy band of holes; consequently, they govern the variation of energy band gap of $Si/Si_{0.7}Ge_{0.3}$ NPs.**

***Index Terms*—energy band, density of state, electrons, light holes, $Si/Si_{0.7}Ge_{0.3}$ nanopillar, Schrödinger equation, $\vec{k}$ space**

I. Introduction

Silicon nanopillars (Si NPs) are promising for more than Moore applications due to the tunable energy-band profiles compared with the materials of bulk Si [1]. Highly periodical Si NPs have been fabricated by the neutral-beam (NB) etching techniques [2], [3]. A thin SiO_2 layer is formed via an oxygen NB at 573 K under 0.14 Pa. A solution of PEG-ferritin (0.05 mg/ml) in 30 mM ammonium acetate is used to form a uniform coating. The wafer is annealed in oxygen to remove the ferritin protein shell. The surface oxide layer is etched using NF_3/H radicals at 300 K under 40 Pa. The iron oxide and surface oxide are used as masks for etching. Via Cl_2 NB etching, the depth of 90 nm can be formed. We remove the masks and then grow $Si_{0.7}Ge_{0.3}$ by thermal CVD. The fabricated sample before depositing the matrix material has good uniformity and alignment, as shown in Fig. 1(a). In our earlier work, modeling and simulation of the electron and hole energy band in real space were reported [4], [5]. However, finite-element simulation of the 3D Schrödinger equation in real space is a very time-consuming task. In this work, we calculate the energy band by solving the Schrödinger equation in $\vec{k}$ space [6], [7]. We model the structure as a superlattice with periodical boundary conditions on the sidewalls. The conduction- and valence-band edges, cut from Fig. 1(b), are in Fig. 1(c) and the band structure is discussed. To model nonideal etching processes, three different shapes [8], as shown in Figs. 1(d)–(f), are also simulated. The simulation flow for the electronic structure calculation and a schematic plot of the irreducible Brillouin zone (IBZ) are plotted in Fig. 1(g).

This work was supported in part by the Ministry of Science and Technology, Taiwan, under Grant MOST 109-2221-E-009-033, Grant MOST 108-2221-E-009-008, and Grant MOST 108-3017-F-009-001, and in part by the "Center for mmWave Smart Radar Systems and Technologies" under the Featured Areas Research Center Program within the framework of the Higher Education Sprout Project by the Ministry of Education in Taiwan.

II. Computational Model

To calculate the energy states, the 3D Schrödinger equation in real space $r = (x, y, z)$ is given by

$$\nabla[\frac{-\hbar^2}{2m^*}\nabla\vec{\psi}_n(\vec{r})] + V(\vec{r})\vec{\psi}_n(\vec{r}) = E_{n,k}\vec{\psi}_n(\vec{r}), \tag{1}$$

where $\hbar$, m^*, $V(\vec{r})$, $E_{n,k}$, and $\vec{\psi}_n(\vec{r})$ are the reduced Plank's constant, the effective mass, the position-dependent potential energy, quantum energy levels, and the corresponding wave function, respectively. The effective masses of electrons along the transverse and longitudinal direction are setting as $0.19m_0$ ($0.12m_0$) and $0.98m_0$ ($1.14m_0$) for Si ($Si_{0.7}Ge_{0.3}$) [10], respectively. The conduction band edges of Si and $Si_{0.7}Ge_{0.3}$ are 0.56 and 0.575 eV, respectively. Assuming that the structure is periodical, by introducing the Bloch theorem, Eq. (1) can be formulated in $\vec{k}$ space as

$$\begin{aligned}\nabla[\frac{-\hbar^2}{2m^*}\nabla\vec{u}_{n,k}] - \frac{i\hbar^2}{m^*}\vec{k}\cdot\nabla\vec{u}_{n,k}(\vec{r}) + [V(\vec{r}) + \frac{\hbar^2\vec{k}^2}{2m^*}]\vec{u}_k(\vec{r}) \\ = E_{n,k}\vec{u}_{n,k}(\vec{r}).\end{aligned} \tag{2}$$

Furthermore, the density of states per IBZ (DOS) is [9]

$$\begin{aligned}DOS(E) &= \frac{2}{(2\pi)^2}\sum_{n,m}\frac{l_n(E,k_m)}{|\nabla_k E_n(k_m)|} \\ &= \frac{2}{(2\pi)^2}\sum_{n,m} DOS_{n,m}(E),\end{aligned} \tag{3}$$

where the factor 2 is the twofold electron spin degeneracy, $1/(2\pi)^2$ is from the conversion of $\vec{k}$ space summation into integration in energy, and l_n is the length of the individual

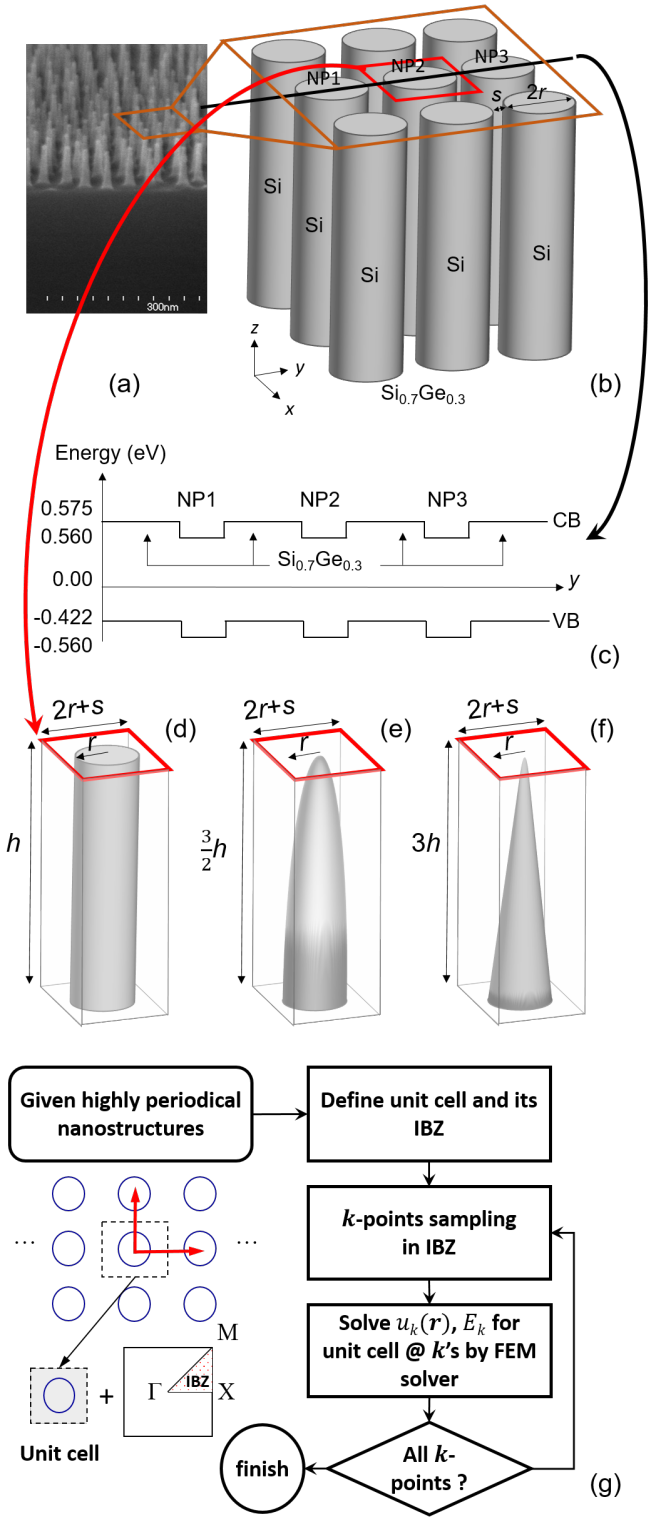

Fig. 1. (a) The side view of the fabricated Si NPs [2], [3]. Schematics of (b) the simulated structure, and (c) the conduction band (CB) and valence band (VB) of Si NPs embedded in $Si_{0.7}Ge_{0.3}$ matrix along y-axis. Note that electrons are confined in the CB of Si NPs while holes are confined in $Si_{0.7}Ge_{0.3}$. To model the nonideal etching processes, three different Si NPs with (d) cylindrical, (e) elliptical, and (f) conical shapes are constructed and simulated by solving Eq. (2) in $\vec{k}$ space, respectively. (g) The simulation flow for the electronic structure calculation for a given highly periodical nanostructure by introducing the concept of IBZ in $\vec{k}$ space. For each sampling point in IBZ, the eigenvalue problem of Eq. (2) is solved.

segments with a constant energy E in the 2D $\vec{k}$ space at sampling point m.

III. Results and Discussion

To verify the computational efficiency of the simulation in $\vec{k}$ space, we first compute the electron ground-state energy in real and $\vec{k}$ spaces by solving Eqs. (1) and (2). As shown in Fig. 2(a), the electron ground-state energy converges to the same result when the number of Si NPs in real space is increased. However, the larger problem size, the longer computational time. More specifically, the calculation of the energy states of a single point in $\vec{k}$ space only takes 25 s; however, to reach the same accuracy, at least 49 Si NPs should be simulated in real space which requires more than 104 s. Figs. 2(b), (c) and (d) show the s-orbit and p-orbit of the Si NP with $r = 5$ nm and $s = 4$ nm for the electrons with an isotropic effective mass along z-, x- and y-direction, respectively. Thus, the Schrödinger equation in $\vec{k}$ space is adopted for the following simulations. The height, radius, separation, and shape effect on the energy band of the Si NPs–$Si_{0.7}Ge_{0.3}$ composite for electrons.

	k space Single point	Real space			
		3x3 NPs	5x5 NPs	7x7 NPs	9x9 NPs
Electron wavefunction distribution	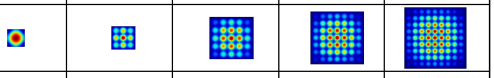				
Normalized Error	--	5.0%	2.5%	0.0%	0.0%

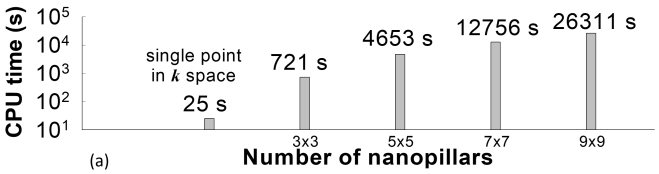

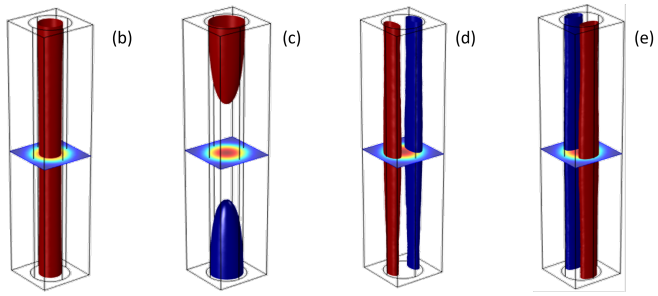

Fig. 2. (a) The computational time of Eq. (1) and (2) with respect to the number of Si NPs, where the case of $r = 5$ nm and $s = 2$ nm is simulated. For the $\vec{k}$ space simulation by Eq. (2), only 25 s are needed at a $\vec{k}$ point; however, to reach the same accuracy of the electron ground-state energy level, at least $7 \times 7 = 49$ Si NPs are needed in real space and the computational time is more than 10000 sec. The (b) s-orbit and p-orbit of the Si NP along (c) z-, (d) x-, and (e) y-direction for electrons with an isotropic effective mass.

A. Height Effect

To understand the height effect of Si NPs on the energy band for electrons, we split three conditions. Fig. 3 shows the electron energy states and DOS calculated from cylindrical Si NPs with the radius of 2 nm, the separation of 5 nm, and the

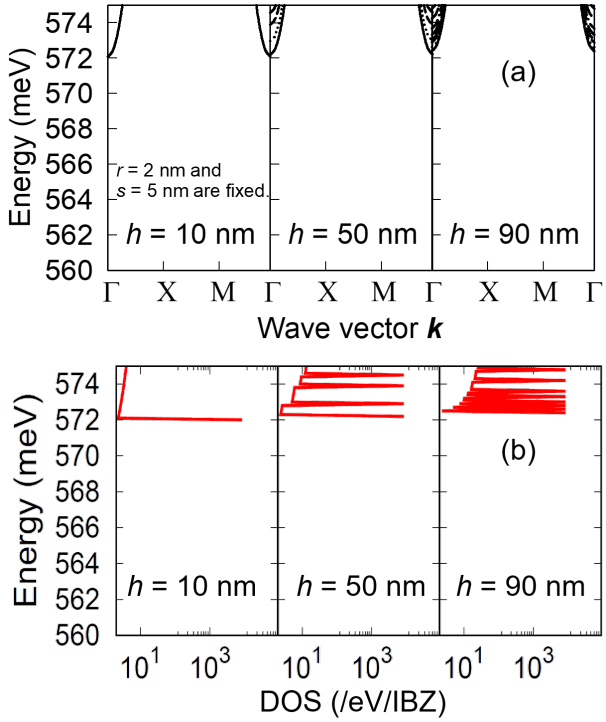

Fig. 3. The (a) electron energy states and (b) density of DOS of the cylindrical Si NPs with the radius of 2 nm and the separation of 5 nm with respect to different heights. The height effect on the ground-state energy is with a little increase as the height of Si NPs are increased; however, it is non-significant. The number of bound states is increased as the height of Si NPs is increased.

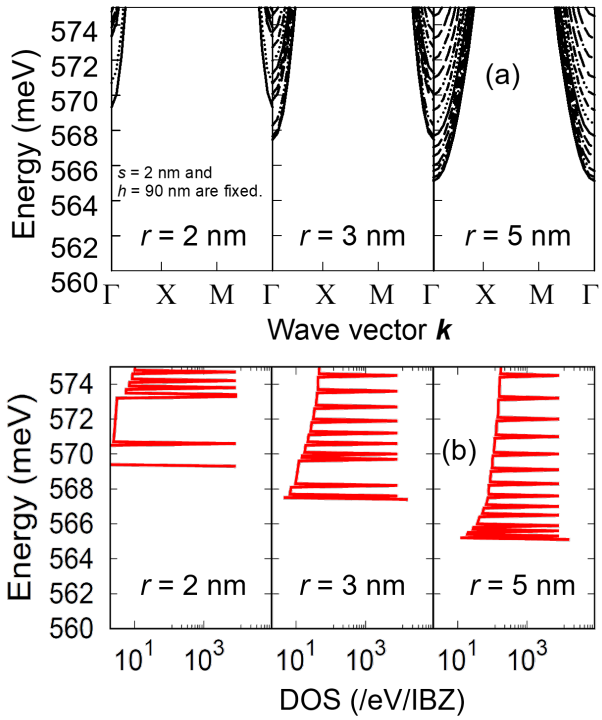

Fig. 4. The (a) electron energy states and (b) DOS of the cylindrical Si NPs with the separation of 2 nm and the height of 90 nm with respect to different radii. As the radius is increased, the wave function is well confined in the Si NPs and lead to a lower ground-state energy.

height of 10, 50, and 90 nm, respectively. The ground-state energy is with a little increase as the height of Si NPs are increased; however, it is insignificant. The number of bound states is increased as the height of Si NPs is increased.

B. Radius Effect

Because the Si NPs is regarded as the potential well to confine the wave function, we fixed the height of Si NPs at 90 nm consistent with our fabrication result and do the energy-band simulation for electrons. Figs. 4(a) and (b) show the electron energy states and DOS of the cylindrical Si NPs with the separation of 2 nm with respect to different radii. As the radius is increased, the wave function is well confined in the Si NPs and lead to a lower ground-state energy.

C. Separation Effect

The separation effect on the electron energy states and DOS of the cylindrical Si NPs with the radius of 2 nm and the height of 90 nm are plotted in Figs. 5(a) and (b). When the separation is small, the potential barrier is thin for electrons; thus, the wave function could penetrate the barrier and lead to a low ground state energy.

D. Shape Effect

Fig. 6(a) shows the influence of shape on energy is negligible; nevertheless, the cylindrical NPs possess the lowest energy among three shapes owing to the best wave function

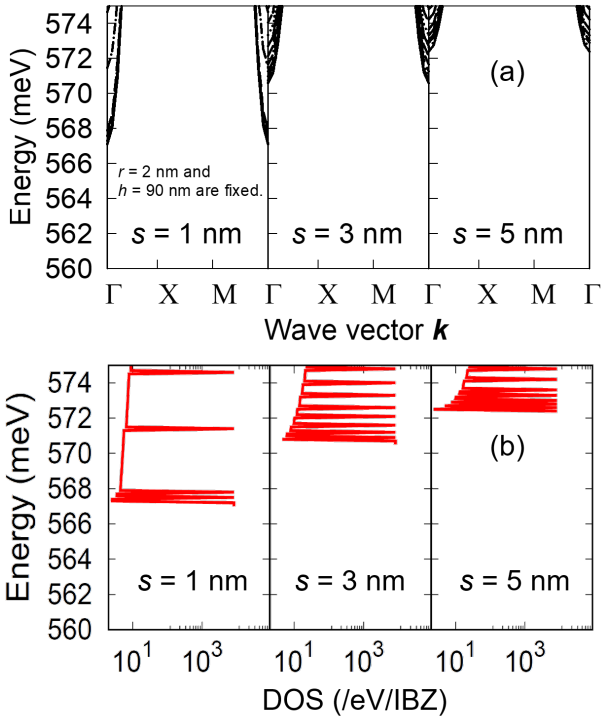

Fig. 5. The (a) electron energy states and (b) DOS of the cylindrical Si NPs with the radius of 2 nm and the height of 90 nm with respect to different separations. As the separation is small, the potential barrier is thin for electrons; thus, the wave function could penetrate the barrier and lead to a low ground state energy.

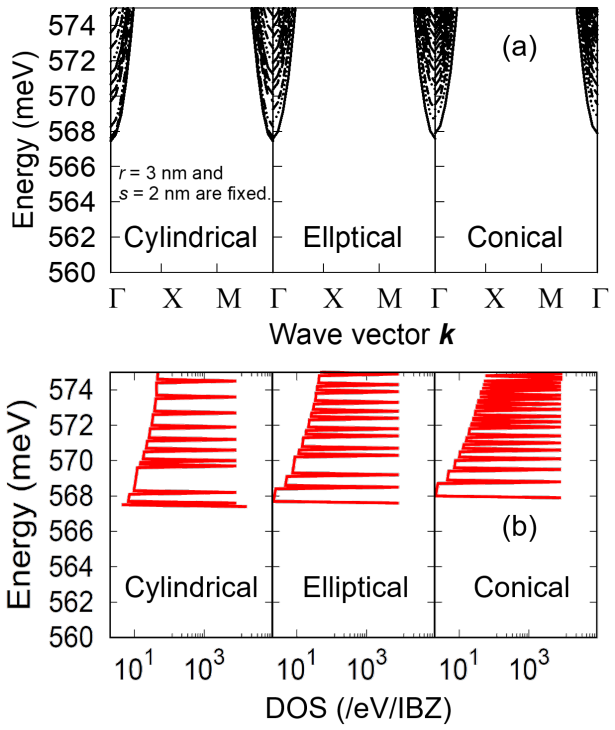

Fig. 6. The (a) electron energy states and (b) DOS of the cylindrical, elliptical, and conical Si NPs with $s = 2$ nm and $r = 3$ nm. The volume is setting as 2544.6 nm^3. As the shape of Si NPs changes from cylinder to cone, the ground-state energy is increased; however, the effect of the shape of Si NPs on the energy band and DOS is marginal owing to high geometry aspect ratio.

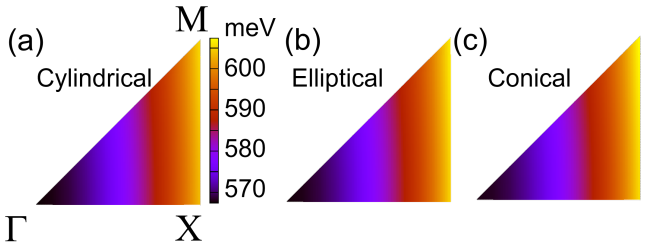

Fig. 7. Plot of the electron ground-state energy on the IBZ for (a) cylindrical, (b) elliptical, and (c) conical Si NPs. All shapes of Si NPs have similar energy distribution owing to similar accommodation structures. At the Γ-valley, the ground-state energy is the lowest.

confinement. As shown in Fig. 6(b), the DOS of the conical NPs is different from others. Figs. 7(a)–(c) show their ground-state-energy distributions on the IBZ. The energy distributions on the IBZ are corresponding to the results in Fig. 6. All shapes of Si NPs have similar energy distribution owing to similar accommodation structures.

We conduct similar simulation for heavy holes and light holes. In contrast with the results of electrons, the radius and separation play crucial role in tuning the energy band of light holes. Especially, not shown here, the separation of Si NPs provides even more significant tunable range on the energy band of light holes. Fig. 8 shows the band gap of Si/Si$_{0.7}$Ge$_{0.3}$

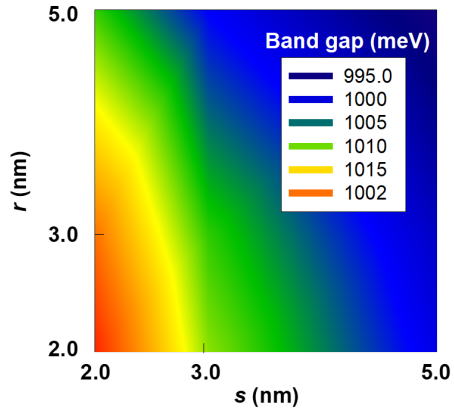

Fig. 8. The band gap of Si/Si$_{0.7}$Ge$_{0.3}$ NPs as a function of the radius and the separation. As the separation is decreased, the band gap becomes large and closed to that of bulk Si because of Si NPs rich in the Si$_{0.7}$Ge$_{0.3}$ matrix.

NPs with respect to different radii and separations. More than 20 meV variation can be altered by changing the separation of Si NPs which is mainly contributed by heavy holes.

IV. Conclusions

In summary, we have performed 3D finite element simulations on highly uniform Si/Si$_{0.7}$Ge$_{0.3}$ NPs for electronic structure calculation. The dependences of energy band and DOS on the heights, radii, separation distances, and shapes of Si NPs have been discussed. The separation of Si NPs plays a key role in tuning the band gap among four factors.

References

[1] N. Neophytou, A. Paul, and G. Klimeck, "Bandstructure effects in silicon nanowire hole transport," IEEE Trans. Nanotechnol., vol. 7, pp. 710–719, Nov. 2008.

[2] A. Kikuchi, A. Yao, I. Mori, T. Ono, and S. Samukawa, "Composite films of highly ordered Si nanowires embedded in SiGe$_{0.3}$ for thermoelectric applications," J. Appl. Phys., vol. 122, p. 165302, Oct. 2017.

[3] M.-H. Chuang, D. Ohori, Y. Li, K.-R. Chou, and S. Samukawa, "Fabrication and simulation of neutral-beam-etched silicon nanopillars," Vacuum, vol. 181, p. 109577, Nov. 2020.

[4] W. Hu, M. Igarashi, M.-Y. Lee, Y. Li, and S. Samukawa, "50% Efficiency Intermediate Band Solar Cell Design Using Highly Periodical Silicon Nanodisk Array," in Tech. Dig. IEDM, San Francisco, CA, Dec. 10–12, 2012, pp. 6.1.1–6.1.4.

[5] W. Hu, M. M. Rahman, M.-Y. Lee, Y. Li, and S. Samukawa, "Simulation study of type-II Ge/Si quantum dot for solar cell applications," J.Appl. Phys., vol. 114, p. 124509, Sep. 2013.

[6] M.-Y. Lee, Y. Li, and S. Samukawa, "Miniband calculation of 3-D nanostructure array for solar cell applications," IEEE Trans. Electron Dev., vol. 62, pp. 3709–3714, Nov. 2015.

[7] M.-Y. Lee, Y. Li, M.-H. Chuang, D. Ohori, and S. Samukawa, "Numerical Simulation of Thermal Conductivity of SiNW–SiGe$_{0.3}$ Composite for Thermoelectric Applications," IEEE Trans. Electron Devices, vol. 67, pp. 2088–2092, May 2020.

[8] Y.-C. Tsai, M.-Y. Lee, Y. Li, and S. Samukawa, "Miniband formulation in Ge/Si quantum dot array," Jpn. J. Appl. Phys., vol. 55, p. 04EJ14, Mar. 2016.

[9] J.-H. Lee, T. Shishidou, and A. J. Freeman, "Improved triangle method for two-dimensional Brillouin zone integrations to determine physical properties," Phys. Rev. B, vol. 66, p. 233102, Dec. 2002.

[10] F. Schaffler, "Silicon-Germanium," in Properties of Advanced Semiconductor Materials: GaN, AlN, InN, BN, SiC, SiGe, M. E. Levinshtein, S. L. Rumyantsev, and M. S. Shur, Eds., Wiley: New York, 2001.